Thermodynamic Contributions for the Incorporation of GTA Triplets within Canonical TAT/TAT and C^+GC/C^+GC Base-Triplet Stacks of DNA Triplexes†

Ana Maria Soto‡ and Luis A. Marky*,‡,§,||

Department of Pharmaceutical Sciences, Department of Biochemistry and Molecular Biology, and Eppley Institute for Cancer Research, University of Nebraska Medical Center, 986025 Nebraska Medical Center, Omaha, Nebraska 68198-6025

Received May 20, 2002; Revised Manuscript Received August 19, 2002

ABSTRACT: Nucleic acid triple helices may be used in the control of gene expression. One limitation of using triplex-forming oligonucleotides as therapeutic agents is that their target sequences are limited to homopurine tracts. To increase the repertoire of sequences that can be targeted, it has been postulated that a guanine can target a thymidine forming a stable GTA mismatch triplet. In this work, we have used a combination of optical and calorimetric techniques to determine thermodynamic unfolding profiles of two triplexes containing a single GTA triplet, $d(A_3TA_3C_5T_3AT_3C_5T_3GT_3)$ (ATA) and $d(AGTGAC_5TCACTC_5TCGCT)$ (GTG), and their control triplexes, $d(A_7C_5T_7C_5T_7)$ (TAT7) and $d(AGAGAC_5TCTCTC_5TCTCT)$ (AG5T). In general, the presence of a GTA mismatch in DNA triplexes is destabilizing; however, this destabilization is greater when placed in a C^+GC/C^+GC base-triplet stack than between a TAT/TAT stack. These destabilizations are accompanied by a reduced unfolding enthalpy of ∼10 kcal/mol, suggesting a decrease in the base stacking contributions surrounding the mismatch. Relative to their corresponding control triplexes, the folding of ATA is accompanied by a lower counterion uptake and a similar proton uptake, while GTG folding is accompanied by an increase in the counterion and proton uptakes. These effects are consistent with the observed decrease in stacking interactions. The overall results indicate that the main difficulty of targeting pyrimidine interruptions is that the decrease in stacking contributions, due to the incorporation of a GTA mismatch, affects the stability of the neighboring base triplets. This suggests that nucleotide analogues that increase the strength of these base-triplet stacks will result in a more effective targeting of pyrimidine interruptions.

The formation of triple helices was first reported in 1957 (*1*), where continuous variation experiments unequivocally indicated that poly A and poly U associate in 1:2 complexes in the presence of divalent cations. However, it was in the 1980s that several groups became interested in these structures and their potential as DNA-targeting agents was recognized (*2*−*5*). Triple helices are formed when a third strand of appropriate sequence binds to the major groove of a DNA duplex (*2*). The formation of triple helices is sequence specific and, therefore, provides a potential way of controlling gene expression (*3*, *4*). Due to their exquisite selectivity, triplexes can be exploited as tools in molecular biology (*2*) or as therapeutic agents (*6*). Triplexes can be classified on the basis of the composition and/or orientation of the third strand. Pyrimidine-rich third strands bind the purine strand of the duplex in the parallel orientation ,while purine-rich third strands bind in the antiparallel orientation (*7*−*9*). Triplexes of the pyrimidine motif are characterized by the formation of T*A·T and C^+*G·C base triplets ("*" and "·" represent Hoogsteen and Watson−Crick base pairing, respectively), as shown in Scheme 1. These triplets allow a regular conformation of the sugar−phosphate backbone because they are isomorphous, i.e., super imposable (*7*).

Recognition of a DNA duplex by the third strand relies in Hoogsteen base paring between the third strand pyrimidines and the duplex purine bases (*10*). Pyrimidine bases present only one hydrogen bond donor or acceptor facing the major groove, resulting in the formation of weaker triplets (*11*). Thus, recognition of the third strand is limited to purine bases, restricting the use of triple helices to homopurine−homopyrimidine tracts (*12*). Much effort has been directed toward identification of nucleotide bases that could target pyrimidine bases. A result of these efforts was the recognition that a third strand guanine could target a thymidine forming a specific and relatively stable G*T·A mismatch triplet (*11*, *13*), Scheme 1. NMR studies have confirmed that a third strand guanine is able to form a hydrogen bond with a thymidine in a T·A base pair (*14*−*18*), and Dnase footprinting studies have shown that two consecutive GTA triplets could afford triple helix formation, even in the absence of a stabilizing triplex-binding ligand (*19*). These studies have suggested that GTA triplets offer a means of bypassing pyrimidine interruptions, thereby increasing the repertoire of sequences that can be targeted using triple helices. However, to exploit GTA triplets for the recognition of DNA sequences, it is important to have clear answers to the

† This work was supported by Grant GM42223 (LAM) from the National Institutes of Health and a Blanche Widaman Fellowship (AMS) from UNMC.

* Corresponding author. Tel: (402) 559-4628. Fax: (402) 559-9543. E-mail: lmarky@unmc.edu.

‡ Department of Pharmaceutical Sciences, University of Nebraska Medical Center.

§ Department of Biochemistry and Molecular Biology, University of Nebraska Medical Center.

|| Eppley Institute for Cancer Research, University of Nebraska Medical Center.

10.1021/bi026166p CCC: $22.00
Published on Web 09/20/2002

Scheme 1: Structure of the TAT, C^+GC, and GTA base triplets

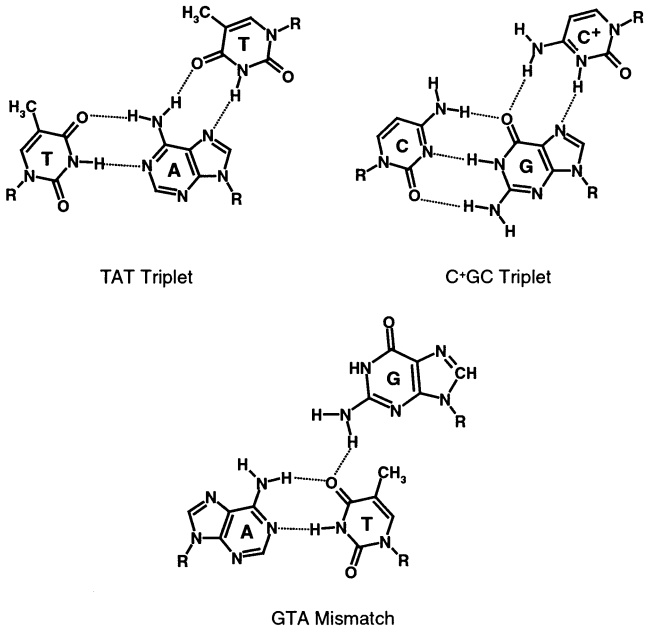

following questions. What forces contribute to the stability of this triplet? How do they compare to the forces stabilizing canonical base triplets? How does the neighboring triplets affect the stability of GTA triplets? What is the role of pH and ionic strength in the stability of this triplet? A careful characterization of the energetic contributions to the stability of GTA triplets will not only be useful in their development as modulators of gene expression, but it will also help in the identification of basic principles for the design of nucleotide analogues that could afford improved recognition of pyrimidine interruptions.

In this work, we have used a combination of optical and calorimetric techniques to characterize two intramolecular triplexes containing a GTA triplet between two C^+GC and between two TAT base triplets. We have compared the energetic profiles of these triplexes with those of their corresponding control triplexes, which contain a canonical TAT triplet in place of the GTA mismatch. Our results show that, relative to the control triplexes, the inclusion of a GTA mismatch is destabilizing. The destabilization is accompanied by a reduced folding enthalpy, suggesting a decrease in base stacking contributions. Moreover, the uptake of protons and counterions observed in these triplexes are consistent with a decrease in stacking interactions. Our overall results suggest that the incorporation of a GTA mismatch could be tolerated when placed between two TAT triplets.

MATERIALS AND METHODS

Materials. All oligonucleotides were synthesized, HPLC purified, and desalted by the Synthetic Core Facility of the Eppley Research Institute at UNMC. The concentration of the oligomer solutions was determined at 260 nm and 80 °C using the following molar extinction coefficients, in mM^{-1} cm^{-1} of strands: $^{5'-}d(A_3TA_3C_5T_3AT_3C_5T_3GT_3)^{-3'}$, 278.6; $^{5'-}d(AGTGAC_5TCACTC_5TCGCT)^{-3'}$, 210.9; $^{5'-}d(A_7C_5T_7C_5T_7)^{-3'}$, 273.1; and $^{5'-}d(AGAGAC_5TCTCTC_5TCTCT)^{-3'}$, 209.7. These values were calculated by extrapolation of the tabulated values of the dimmers and monomer bases at 25 °C (*20*) to high temperatures, using a procedure reported earlier (*21*). Buffer solutions consisted of 10 mM sodium cacodylate or 10 mM sodium phosphate, adjusted to different sodium concentrations and pH with NaCl and HCl, respectively. All molecules and their corresponding designations are shown in Scheme 2.

Scheme 2: Sequences of Triplexes

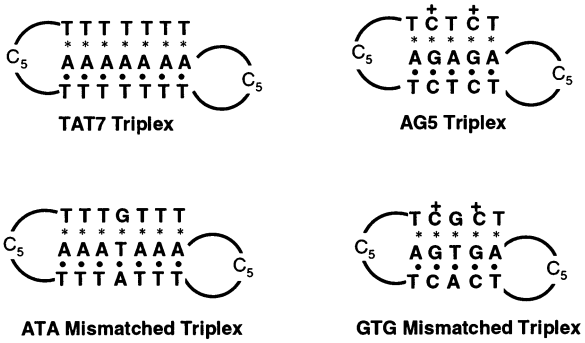

Circular Dichroism (CD).[11] Evaluation of the conformation of each triplex was obtained by simple inspection of their CD spectrum. These spectra were obtained on an AVIV Circular Dichroism Spectrometer Model 202-SF (Lakewood, NJ), using a 10 mm quartz cuvette. All spectra were collected at 0 °C, between 200 and 400 nm, using a wavelength step of 1 nm. The reported spectra represent the average of at least two scans.

Temperature-Dependent UV Spectroscopy (UV Melts). Absorbance versus temperature profiles (melting curves) for each duplex and triplex were measured at 260 nm using a thermoelectrically controlled Aviv 14-DS spectrophotometer and as a function of strand, pH, and salt concentration. The temperature was scanned at a heating rate of ~0.6 °C/min. These melting curves allow us to measure transition temperatures, T_M, which are the midpoint temperatures of the order−disorder transition of the duplexes and triplexes, van't Hoff enthalpies, ΔH_{vH}, using a two-state transition approximation as reported previously (*22*), and the thermodynamic release of protons and counterions, Δn_{H^+} and Δn_{Na^+}, respectively.

Differential Scanning Calorimetry (DSC). Excess heat capacity as a function of temperature profiles for the helix coil transition of each triplex were measured with a Microcal MC-2 or VP differential scanning calorimeters (Northampton, MA), using two cells. The sample cell containing 1.6 mL (MC-2) or 0.8 mL (VP) of oligomer solution and the reference cell filled with the same volume of buffer solution were heated from 0 to 90 °C at a heating rate of 0.75 °C/min. Analysis of the resulting thermograms, using procedures described previously (*22*), yields standard thermodynamic profiles (ΔH_{cal}, ΔS_{cal}, and ΔG°_{cal}) and model dependent van't Hoff enthalpies, ΔH_{vH}, for the transition of each triplex.

RESULTS

UV *Melting Curves*. UV melting experiments were conducted at different salt and pH conditions and were used to characterize the helix−coil transition of each triplex. The UV melts of each triplex in 10 mM sodium cacodylate buffer,

[1] Abbreviations: CD, circular dichroism; DSC, differential scanning calorimetry.

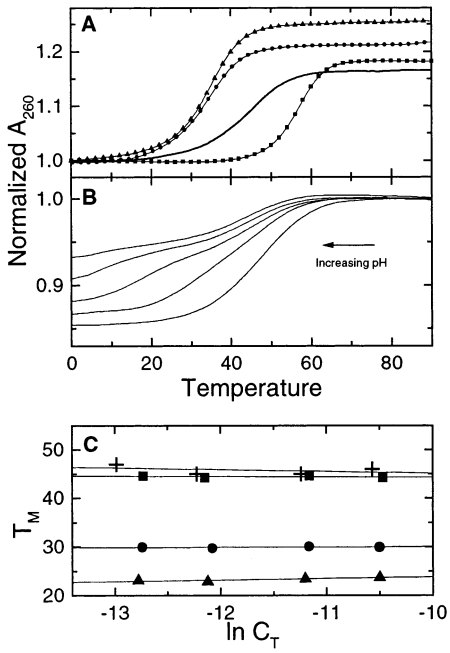

FIGURE 1: (A) UV melts of TAT7 (▲), ATA (●), AG5T (■), and GTG (solid line) in 10 mM sodium cacodylate buffer, pH 5.2. (B) UV melts of GTG as a function of pH in 10 mM sodium cacodylate, 200 mM sodium chloride. (C) T_M dependence on strand concentration of TAT7 (▲), ATA (●), in 10 mM sodium phosphate, pH 7.0, and sodium concentrations of 16 and 116 mM, respectively, and of AG5T (■) and GTG (+) in 10 mM sodium cacodylate pH 6.2 and 5.2, respectively.

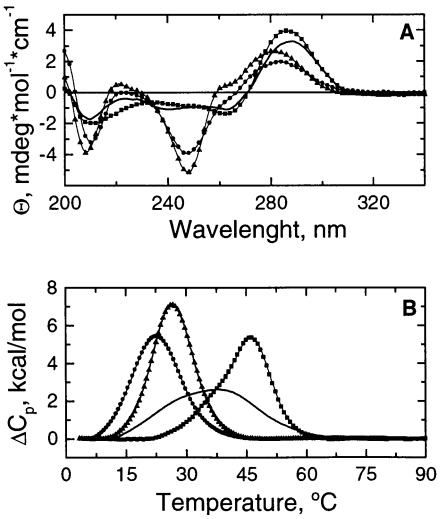

FIGURE 2: (A) Circular dichroism spectra of TAT7 (▲) and ATA (●) in 10 mM sodium phosphate at pH 7 and of AG5T (■) and GTG (—) in 10 mM sodium cacodylate at pH 6.2 and 5.2, respectively. (B) DSC curves of TAT7 (▲) and ATA (●) in 10 mM sodium phosphate at pH 7 and of AG5T (■) and GTG (—) in 10 mM sodium cacodylate at pH 6.2.

pH 5.2, are shown in Figure 1a. Above 10 °C, all melting curves follow the characteristic sigmoidal behavior of the unfolding of a nucleic acid. The curves of the "GTA triplexes" (triplexes containing GTA mismatches) exhibit a decrease in hyperchromicity and are shifted to the left, relative to their corresponding control triplexes. This indicates that the incorporation of a GTA triplet decreases the stability of a triplex. This effect is more pronounced in the case of GTG, suggesting that the presence of a GTA mismatch is more destabilizing when surrounded by C^+GC triplets. ATA and TAT7 exhibit monophasic transitions under all conditions. In contrast, GTG and AG5T exhibit monophasic or biphasic transitions, depending on solution conditions. At low sodium concentrations and acidic pH, these triplexes exhibit monophasic transitions, while at basic pH and high sodium concentrations, we observed biphasic transitions. The UV melts of GTG at constant sodium concentrations of 210 mM and over a pH range of 5.2−7.2 are shown in Figure 1b and illustrate this effect. This behavior is consistent with previous observations (*23*) and reflects the opposite effects of sodium ions and protons in the stability of C^+GC triplets. Closer inspection of Figure 1b indicates that, at this sodium concentration, GTG can only form a triplex below pH 6.2. This is in contrast with AG5T, which forms a triplex even at pH 7.2 and suggests that the presence of a GTA mismatch affects the protonation of the third strand cytosines of the neighboring base triplets. Similar experiments at sodium concentrations of 10 mM (data not shown) indicate that GTG can form a triplex below pH 6.7, illustrating the stabilizing effect at low ionic strengths over triplexes containing C^+GC triplets (*23*). UV melts at different total strand concentrations were conducted to determine both the dependence of T_M on strand concentration and associated van't Hoff enthalpies from analysis of their shape. The T_M dependences on strand concentration for the unfolding of each molecule are shown in Figure 1c. Over a 12-fold concentration range, the T_M of each molecule is independent of strand concentration, confirming the formation of intramolecular structures. We used monophasic UV melts and the relationship $\Delta H_{vH} = 4RT_M^2\,\partial\alpha/\partial T$ (*22*) to calculate ΔH_{vH} values of −51 (TAT7), −38 (ATA), −52 (AG5T), and −35 kcal/mol (GTG). These enthalpy values represent the average of at least seven determinations and were found to be independent of pH or sodium concentration.

Circular Dichroism. The CD spectra of each molecule are shown in Figure 2a. TAT7 and ATA exhibit the typical spectra of molecules in the B conformation, with a positive band (∼278 nm) of similar magnitude than the negative band (∼245 nm). AG5T and GTG can also be classified as molecules in the B conformation, although their spectra present some deviations from the typical B conformation, including an overall shift of the spectra toward higher wavelengths. These deviations may results from the presence of protonated cytosines in the stem of these molecules. Comparison of the spectra of the "GTA triplexes" and their corresponding control triplexes indicates that the presence of a GTA mismatch decreases the intensity of each spectrum but has no effect in the overall shape of the spectra. This indicates that the incorporation of a single GTA mismatch does not impose major distortions in the overall conformation of the triplex.

Differential Scanning Calorimetry. Typical DSC melting curves for the unfolding of each oligonucleotide are shown in Figure 2b. DSC experiments were conducted at pH 7 and different sodium concentrations (ATA & TAT7) or at constant sodium concentration of 10 mM and different pH values (AG5T). GTG was only studied at pH 6.2 and 10 mM NaCl because this triplex could not form at higher pH and is greatly destabilized at higher sodium concentrations. Under the conditions of our DSC experiments, TAT7, ATA, and AG5T unfold in monophasic non-two-state transitions. In contrast, GTG exhibit nonsymmetric DSC curves, which

Table 1: Thermodynamic Profiles for the Formation of Triplexes at 5 °C

pH	[Na^+], mM	T_M, °C	ΔH_{cal}[a], kcal/mol	$\Delta G°$ [a], kcal/mol	$T\Delta S_{cal}$[a], kcal/mol	ΔH_{vH}[a], kcal/mol	Δn_{Na^+} [b], per triplex	Δn_{H^+} [c], per triplex
				TAT7				
7	16	23.2	−93.9	−5.8	−88.1	−53	−3.50	−1.51
	116	34.8	−92.9	−9.0	−83.9	−49	(−2.44)	(−1.10)
	1116	53.8	−85.3	−12.7	−72.6	−58		
				ATA				
7	16	20.0	−83.4	−4.3	−79.1	−45	−2.96	−1.57
	116	27.9	−83.6	−6.4	−77.2	−37	(−1.47)	(−1.04)
	1116	46.2	−76.0	−9.8	−66.2	−44		
				AG5T				
7	16	29.3	−69.3	−5.6	−63.7	−49	0.97	−2.68
6.2	10	43.0	−84.8	−10.2	−74.6	−53	(−0.10)	(−4.07)
				GTG				
7	–	–	–	–	–	–	–	−3.66
6.2	10	38.0	−74.3	−7.9	−66.4	−28	(−0.25)	(−5.90)

[a] Experiments were conducted in 10 mM sodium phosphate buffer pH 7.0 or 10 mM sodium cacodylate buffer, pH 6.2. ΔH_{vH} are obtained from the shape of calorimetric melting curves. [b] Experiments were conducted in 10 mM sodium cacodylate buffer, adjusted to different sodium concentrations with NaCl, and at constant pH values of 7.2 or 5.2 (values in parentheses). [c] Experiments were conducted in 10 mM sodium cacodylate buffer, adjusted to different pH values with HCl, and at constant sodium concentrations of 10 or 210 mM (values in parentheses). T_Ms are within 0.5 °C, ΔH_{cal} within 3%, $\Delta G°$ and $T\Delta S$ within 5%, ΔH_{vH} within 10%, and Δn_{Na^+} and Δn_{H^+} within 6%.

may indicate the presence of two transitions with different T_M values. The thermodynamic profiles for the folding of each triplex at 5 °C were determined from DSC experiments and are summarized in Table 1. The ΔH_{cal} and ΔS_{cal} parameters were measured directly using the equations: $\Delta H_{cal} = \int \Delta C_p{}^a \partial T$ and $\Delta S_{cal} = \int (\Delta C_p{}^a/T) \partial T$, where $\Delta C_p{}^a$ is the anomalous heat capacity during the unfolding process. The free energy at 5 °C, $\Delta G°_{278}$, is obtained from the Gibbs equation: $\Delta G°_{278} = \Delta H_{cal} - T\Delta S_{cal}$. In addition, van't Hoff enthalpies, calculated from the shape of the calorimetric curves, are shown in Table 1. The resulting enthalpy values are similar to the ones obtained from analysis of the UV melting curves. The large difference between van't Hoff and calorimetric enthalpies obtained for each triplex indicates that these molecules unfold in non-two-state transitions and suggests the presence of two coupled transitions with similar T_M values. Inspection of Table 1 indicates that the folding of each triplex or duplex at 5 °C is accompanied by a favorable free energy term resulting from the compensation of favorable enthalpy and unfavorable entropy terms. These favorable enthalpy terms correspond to the formation of base-pair stacking interactions, while the unfavorable entropy terms arise from contributions of the unfavorable ordering of strands and the uptake of counterions, protons and water molecules. The stability of ATA and TAT7 increases as the sodium concentration increases. This is due to the better screening of the negatively charged phosphates at higher ionic strengths. The stabilizing effect of sodium is more pronounced in the case of TAT7, suggesting that this triplex has a higher charge density parameter than ATA. In addition, the enthalpy values of TAT7 and ATA appear to be independent of sodium concentrations but decrease at salt concentrations of 1.1 M. The stability of AG5T increases with decreasing pH, which is consistent with previous reports (*23*) and indicates the requirement of cytosine protonation in the formation of C^+GC triplets. Table 1 shows that the GTA triplexes are less stable than their corresponding control triplexes and that the overall destabilization is more pronounced in the case of GTG. Therefore, a GTA triplet is more destabilizing when incorporated between two C^+GC triplets. Furthermore, the control triplexes unfold with larger enthalpies compared with the GTA triplexes, suggesting that the incorporation of a GTA triplet causes a decrease in stacking interactions.

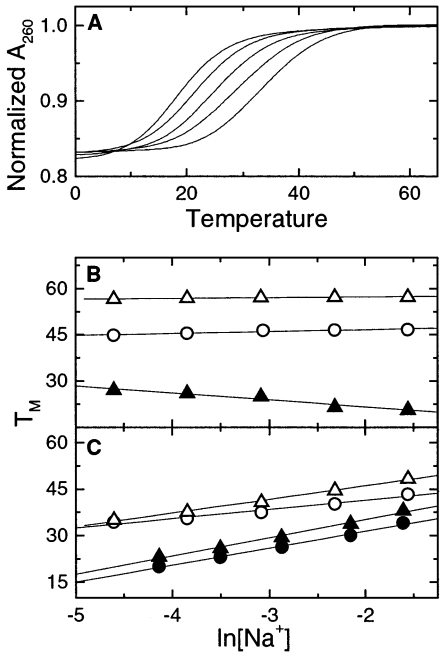

FIGURE 3: (A) UV melting curves of ATA over a NaCl concentration range of 16−200 mM in 10 mM sodium phosphate, pH 7.0, at constant strand concentration of 5 μM. (B) T_M dependence on salt concentration at pH 7 (solid) and pH 5.2 (open) for AG5T (triangles) and GTG (circles). (C) T_M dependence on salt concentration at pH 7 (solid) and pH 5.2 (open) for TAT7 (triangles) and ATA (circles).

Thermodynamic Release of Counterions. UV melting curves at several salt concentrations and the T_M dependence on salt concentration are shown in Figure 3. The thermodynamic release of counterions, Δn_{Na^+}, is determined from the equation $\Delta n_{Na^+} = 1.11(\Delta H_{cal}/RT_M{}^2)(\partial T_M/\partial \ln[Na^+])$ (*24*) where 1.11 is a proportionality constant for converting concentrations into ionic activities; the first term in parentheses is obtained in DSC melting experiments, R is the

universal gas constant, and the second term corresponds to the slope of T_M versus ln [Na^+] plots. These $\Delta n_{Na}{}^+$ values were calculated from the slopes of the T_M dependence on sodium at pH 5.2 or 7.2 and the enthalpies values obtained at low sodium concentration and pH 7 (TAT7, ATA, and AG5T) or pH 6.2 (GTG and AG5T). The resulting $\Delta n_{Na}{}^+$ values are summarized in Table 1. Under all pH conditions, ATA and TAT7 uptake counterions; this is in agreement with a previous report (*25*) and reflects the higher charge density of the folded molecules relative to the random coil states at pH 6.2 (GTG and AG5T). The resulting $\Delta n_{Na}{}^+$ values are summarized in Table 1. Under all pH conditions, ATA and TAT7 uptake counterions, in agreement with a previous report (*25*) and reflecting the higher charge density of the folded molecules relative to the random coil states. However, the uptake of sodium ions at pH 5.2 is smaller than that at pH 7.2, consistent with an earlier report (*23*), and probably reflects the decrease in the negative charge density due to protonation of the cytosine loops (*23*). At either pH, ATA has a smaller uptake of counterions than TAT7, indicating that the presence of a GTA mismatch yields a decrease in the charge density parameter. The decrease in uptake of counterions is more evident at pH 5.2, indicating a further reduction in charge density at low pH. At pH 7.2, the folding of AG5T releases counterions, perhaps due to the protonation of the third strand cytosines, which exclude sodium from the stem of this triplex. The release or uptake of counterions of GTG was only analyzed at pH 5.2 because this triplex does not form completely at pH 7. At pH 5.2, GTG and AG5T uptake very small amounts of counterions; this uptake is somehow larger for GTG, suggesting that the incorporation of a GTA mismatch results in a slight increase in their charge density parameter.

Thermodynamic Release of Protons. UV melting curves at several pH values and the T_M dependence on pH are shown in Figure 4. The thermodynamic release of protons, $\Delta n_{H}{}^+$, is determined from the equation $\Delta n_{H}{}^+ = -0.434(\Delta H_{cal}/RT_M{}^2)(\partial T_M/\partial pH)$ (*26*, *27*), where 0.434 is a proportionality constant for converting decimal logarithms into natural logarithms, the first term in parentheses is obtained in DSC experiments, and the $\partial T_M/\partial pH$ term corresponds to the slope of T_M versus pH plots. The resulting $\Delta n_{H}{}^+$ values are shown in Table 1. TAT7 and ATA uptake small amounts of protons, probably reflecting the protonation of the cytosine loops. Since both molecules have identical constrained cytosine loops, there are no differences in the counterion uptake of these molecules. AG5T and GTG uptake larger amounts of protons, due to the protonation of their stem and loop cytosines. The proton uptake of these triplexes increases as the sodium concentration increases, suggesting that the presence of sodium decreases the pK_a of both stem and loop cytosines. The GTG triplex has a larger proton uptake than the AG5T triplex. This suggests that the presence of a GTA mismatch decreases the pK_a of the cytosines in the neighboring base triplets. This effect is more pronounced at high sodium concentrations, indicating that the cytosines bases in GTG are more susceptible to the effects of sodium over the pK_a than the cytosines in AG5T.

DISCUSSION

All molecules were design to fold into intramolecular structures. We chose to work with intramolecular triplexes because they are more stable than their bimolecular and trimolecular counterparts, due to a lower entropy cost. In addition, they can form even at low sodium concentrations, enabling us to study their properties in a variety of solution conditions. This is in contrast to intermolecular triplexes, which can only form at very high salt concentrations or in the presence of divalent cations. As shown in Figure 1c, the T_M of all triplexes is independent of strand concentration, confirming the exclusive formation of intramolecular structures.

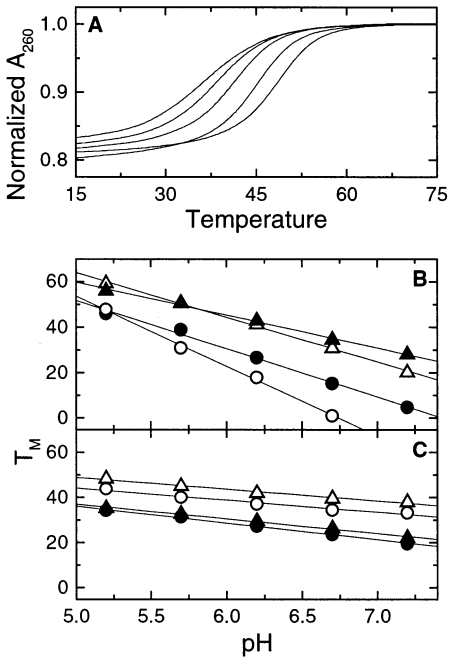

FIGURE 4: (A): UV melting curves of TAT7 over a pH range of 5.2−7.2 in 10 mM sodium cacodylate, 200 mM NaCl, at constant strand concentration of 5 μM. (B) T_M dependence on pH at constant sodium concentrations of 10 mM (solid) or 210 mM (open) for AG5T (triangles) and GTG (circles). (C) T_M dependence on pH at constant sodium concentrations of 10 mM (solid) or 210 mM (open) for TAT7 (triangles) and ATA (circles).

We have incorporated a GTA triplet in two different environments: between two TAT triplets and between two C^+GC triplets. GTG contains a GTA mismatch placed between two C^+GC triplets, while its control triplex, AG5T, contains a TAT triplet in place of the mismatch. Similarly, ATA incorporates a GTA mismatch between two TAT triplets, while TAT7 contains a TAT base triplet in place of the mismatch. The comparison between control and mismatched triplexes will allow us to determine the energetic consequences resulting from inversion of an AT base pair and subsequent recognition of a pyrimidine base with a guanine base.

Our initial UV melting experiments indicated that the presence of a GTA mismatch is destabilizing and that this destabilization is greater when the GTA triplet is incorporated between two C^+GC triplets. The melting curves in Figure 1a also show that the hyperchromicity of the control triplexes is greater than that of the mismatches. This suggests that the incorporation of a GTA mismatch causes a decrease in stacking interactions, yielding an increased exposure of the aromatic bases to the solvent.

Circular Dichroism. The similarity between the CD spectra of the GTA triplexes and their control triplexes indicates that

the presence of a single GTA mismatch does not alter the overall conformation of these triplexes. The bands in the CD spectra of the "GTA triplexes" are of lower magnitude, with respect to their control triplexes. This suggests a decrease in stacking interactions around the mismatch, which results in an overall decrease of the number of residues contributing to the ellipticity of the molecule. As previously observed (*23*), the CD spectra of the triplexes containing protonated cytosines deviate from the spectrum of the typical B conformation. These deviations may results from the presence of protonated cytosines in the stem of these molecules, which may alter the electronic properties of the cytosine to which they are attached and of the neighboring bases.

Differential Scanning Calorimetry. Under the conditions of our DSC experiments, TAT7 and ATA unfold in monophasic, non-two-state transitions, suggesting the presence of two coupled transitions with similar T_M values. Indeed, these DSC curves can be deconvoluted (panel A of Figure 1S, Supporting Information) into two transitions with similar T_M. AG5T and GTG exhibit nonsymmetric DSC curves, suggesting the presence of two transitions with different T_M values. Deconvolution of the DSC curves indicates that each transition can be decomposed into two transitions with a T_M difference of 4 and 13 °C (panel B of Figure 1S), respectively. Inspection of Table 1 indicates that the incorporation of a GTA mismatch destabilizes a triplex. The destabilization is accompanied by a decreased enthalpy of formation, indicating that the presence of a GTA mismatch results in a decrease in stacking interactions. This is consistent with the decrease in hyperchromicity observed in the melting curves and the decrease in ellipticity observed in our CD experiments. The decrease in stacking interactions may arise from the weaker interaction between the third strand guanine and its thymidine target due to the presence of a single hydrogen bond. In addition, the presence of a guanine base in the middle of a homopyrimidine third strand may impose structural distortions that may also contribute to the observed decrease in stacking interactions. Moreover, NMR studies have also shown that the presence of a purine in a homopyrimidine segment necessitates local structural readjustments, which effectively tilt the guanine out of the plane of the TA base pair (*15*). Furthermore, the presence of the thymidine methyl group may also contribute to the orientation of guanine relative to its target base pair. To this effect, NMR studies have suggested that the third strand guanine needs to be rotated away from the center of the helix in order to avoid steric clash with the methyl group of its thymidine target (*15*). The stability (T_M and $\Delta G°$) of ATA and TAT7 increases as the sodium concentration increases. This is indicative of a better screening of the negatively charged phosphates at higher ionic strengths. In addition, their enthalpy values appear to be independent of sodium concentrations, consistent with the negligible heat contributions of cation binding (*28*). These enthalpies decrease only at very high sodium concentrations, which is probably induced by the effect of high sodium concentrations on the properties of the solvent. Comparison of the thermodynamic profiles of TAT7 and ATA indicates that the presence of a GTA mismatch between two TAT triplets is destabilizing under all salt concentrations. Moreover, the destabilization seems to increase as the ionic strength increases. This is a consequence of the decrease in stacking interactions, which results in a decrease in charge density around the mismatch. The stabilizing effect of sodium ions will be more pronounced for a molecule with higher charge density, accounting for the higher stabilization of TAT7. The stability of AG5T increases with decreasing pH, in good agreement with previous reports (*23*), and indicates the requirement of cytosine protonation for the formation of C^+GC triplets. Comparison of the thermodynamic profiles of GTG and AG5T at pH 6.2 shows that the presence of a GTA mismatch between two C^+GC triplets is also destabilizing and that this destabilization arises from a lower enthalpy contribution. To further analyze the effect of a GTA mismatch, we have calculated the differential thermodynamic profiles for the incorporation of a GTA mismatch in these two environments, and the resulting profiles are summarized in Table 2.

Table 2: Differential Profiles for the Formation of ATA and GTG at Low Sodium Concentrations

triplex	$\Delta\Delta G$, kcal/mol	$\Delta\Delta H$, kcal/mol	$\Delta(T\Delta S)$, kcal/mol	$\Delta\Delta n_{Na^+}$ (per triplex)	$\Delta\Delta n_{H^+}$ (per triplex)
ATA	1.5	10.5	9.0	0.54	−0.06
GTG	2.3	10.5	8.2	−0.15	−0.98

Table 2 indicates a similar decrease in the enthalpy of formation of ATA and GTG with respect to their corresponding control triplexes, suggesting a similar decrease in stacking interactions. This is expected because the enthalpy contribution for the formation of a TAT/TAT or C^+GC/C^+GC base-triplet stacks is very similar and equal to −23 kcal/mol (*23*). Therefore, the incorporation of a GTA lesion into base-triplet stacks with similar heat contributions should yield similar enthalpic destabilizations. Table 2 also shows that the incorporation of a GTA mismatch between two C^+-GC triplets is more destabilizing (in terms of T_M and $\Delta G°$) than between two TAT triplets. This is in good agreement with previous reports (*29*), and it has been suggested that this increased stability is due to the formation of an additional hydrogen bond between one of the guanine's amino protons and the O4 carbonyl of a duplex thymidine in a neighboring triplet (*15*).

Thermodynamic Release of Counterions. Under all pH conditions, ATA and TAT7 uptake counterions, illustrating the higher charge density of the folded molecules relative to the unfolded states. Their uptake of sodium ions at pH 5.2 is smaller than that at pH 7.2, consistent with previous reports (*23*) and reflecting the decrease in negative charge density due to protonation of the cytosine loops (*23*). At either pH, the uptake of counterions of ATA is smaller that the uptake of counterions of TAT7, suggesting that the presence of a GTA mismatch results in a decrease in negative charge density. This corresponds to the observed decrease in stacking interactions, which may yield an increased distance between the phosphates around the mismatch. This is also in good agreement with the increased stabilization of TAT7 at higher sodium concentrations, as observed in the DSC curves. Closer analysis of Table 1 indicates that the uptake of counterions of ATA, relative to TAT7, is further decreased at pH 5.2. Indeed, the difference in the uptake of counterions between ATA and TAT7 is 0.54 at pH 7.2 and 0.97 at pH 5.2. This indicates that, relative to TAT7, the negative charge density of ATA is further decreased at pH 5.2, suggesting the protonation of the adenine in the TA

target base pair, which may be exposed to the solvent to a greater extent that its AT counterpart in TAT7. Alternatively, the additional decrease in charge density of ATA at low pH may be the result of a greater impact of the protonated cytosine loops over ATA, due to its already low charge density parameter. In contrast, GTG exhibits a small increased uptake of counterions of 0.15 relative to AG5T, which may be within experimental uncertainty rather than reflecting a real trend. Nevertheless, if this trend is real, it indicates that the presence of a GTA mismatch increases the charge density of the folded GTG triplex. This correlates well with the decrease in stacking interactions around the mismatch, which will increase the distance between the protonated cytosines, allowing this triplex to tolerate better the presence of sodium ions around the stem.

Thermodynamic Release of Protons. TAT7 and ATA uptake small amounts of protons, probably reflecting the protonation of the cytosine loops. Since the presence of a mismatch in the middle of the triplex stem is not expected to alter the conformation of the loops, there should be no differences in the uptake of protons between these triplexes. Indeed, we do not observe differences in the proton uptake of these molecules. This further confirms that the observed uptake of protons in these triplexes is mainly due to protonation of the cytosine loops. The similar proton uptakes observed for ATA and TAT7 argues against the protonation of a duplex adenine in ATA at low pH. This suggests that the large decrease in charge density of ATA observed at pH 5.2 is mainly due to the higher impact of the positively charged loops on a molecule having an already low charge density. On the other hand, AG5T and GTG uptake larger amounts of protons, due to the simultaneous protonation of cytosines in both stem and loop. The uptake of protons of GTG is larger than that of AG5T. This suggests that the presence of a GTA mismatch decreases the pK_a of the cytosines in the neighboring base triplets. This decrease in pK_a may be explained by the decrease in stacking interactions around the mismatch, which results in a larger exposure of the third strand cytosines to the solvent. The pK_a of a cytosine that is fully exposed to the solvent is around 4.6 (*30*), while a cytosine fully stacked into the helix has a pK_a of ~7.4 (*31*). A consequence of this pK_a decrease is that the protonation of the third strand cytosines is induced at a lower pH, accounting for the low pH requirement for the formation of the GTG triplex. At this lower pH, the fraction of loop cytosines that are protonated increases, resulting in a higher uptake of protons.

The uptake of protons of AG5T and GTG increases as the sodium concentration increases. This is in good agreement with previous reports (*23*) and suggests that the presence of sodium ions around the positively charged cytosines (stem and loop) decreases their pK_a. One possible explanation is that the presence of sodium ions excludes positive charges from the stem of these triplexes, reducing the protonation of cytosines. Table 1 indicates that the uptake of protons of GTG relative to AG5T is much larger at higher sodium concentrations. This indicates that sodium has a more pronounced effect in the pK_a of the cytosines of the GTG triplex. This may be consistent with the decrease in stacking interactions, which results in an increased charge density parameter and a higher occupancy of sodium ions in the stem of this triplex. The higher concentration of sodium ions around the third strand cytosines further reduces their pK_a, inducing protonation of the third strand cytosines at the lower pH, at which the fraction of protonated loop cytosines increases. This correlates well with the lower pH requirement for the formation of GTG at higher sodium concentrations and with the increased charged density of GTG with respect to AG5T.

CONCLUSION

We used a combination of spectroscopic and calorimetric techniques to determine complete thermodynamic profiles accompanying the folding of intramolecular triplexes containing a GTA mismatch in two different base triplet stacking environments. The presence of a GTA mismatch does not alter the overall conformation of a triplex; however, its single incorporation is destabilizing. This destabilization results from a decrease of favorable enthalpy contributions, which indicates that the incorporation of a GTA mismatch is accompanied by a decrease in stacking interactions. Furthermore, the overall uptake of protons and counterions involved in the formation of GTA-containing triplexes are consistent with the observed decrease in stacking interactions. Furthermore, the incorporation of a GTA mismatch is more destabilizing when placed between two C^+GC base triplets. The higher stability provided by the TAT/TAT environment may be due to the formation of an additional hydrogen bond between the third strand guanine and a thymidine in a neighboring TAT triplet.

The overall results indicate that a GTA triplet may provide a useful way of targeting a thymidine interruption that occurs between two adenines in a homopurine stretch. The recognition of a thymidine between two guanines continues to be a challenge. However, our results suggest that the main difficulty of using a GTA triplet to target a thymidine between guanines is that the decrease in stacking interactions results in a decreased pK_a of the neighboring C^+GC base triplets. This suggests that cytosine analogues that increase the intrinsic pK_a of cytosine may be useful in the recognition of pyrimidine interruptions. Furthermore, strengthening of the base-triplet stacks surrounding a mismatch may be taken as a general principle for the recognition of pyrimidine interruptions. We speculate that replacement of TAT and C^+GC base triplets with nucleotide analogues that increase the strength of these base-triplet stacks should yield a more effective targeting of a pyrimidine interruption. Several nucleotide analogues may be able to trigger such reinforcement, including 5′-propyn-1-yl deoxyuridine, 5′-methyl deoxycytosine, and 5′-propyn-1-yl deoxycytosine.

SUPPORTING INFORMATION AVAILABLE

Deconvolution anaysis of the DSC melting profiles. This material is available free of charge via the Internet at http://pubs.acs.org.

REFERENCES

1. Felsenfeld, G., David, R. D., and Rich, A. (1957) *J. Am. Chem. Soc. 79*, 2023−2024.
2. Moser, H. E., and Dervan, P. B. (1987) *Science 238*, 645−650.
3. Maher, L. J., III, Wold, B., and Dervan, P. B. (1989) *Science 245*, 725−730.
4. Helene, C., and Toulme, J. J. (1990) *Biochim. Biophys. Acta 1049*, 99−125.

5. Neidle, S. (1997) *Anti-Cancer Drug Des. 12*, 433−442.
6. Postel, E. H., Flint, S. J., Kessler, D. J., and Hogan, M. E. (1991) *Proc. Natl. Acad. Sci. U.S.A. 88*, 8227−8231.
7. Soyfer, V. N., and Potaman, V. N. (1996) *Triple-Helical Nucleic Acids*, Springer-Verlag, New York.
8. Keppler, M. D., and Fox, K. R. (1997) *Nucleic Acids Res. 25*, 4644−4649.
9. Beal, P. A., and Dervan, P. B. (1991) *Science 251*, 1360−1363.
10. Rajagopal, P., and Feigon, J. (1989) *Nature 339*, 637−640.
11. Best, G. C., and Dervan, P. B. (1995) *J. Am. Chem. Soc. 117*, 1187−1193.
12. Gowers, D. M., and Fox, K. R. (1999) *Nucleic Acids Res. 27*, 1569−1577.
13. Griffin, L. C., and Dervan, P. B. (1989) *Science 245*, 967−971.
14. Radhakrishnan, I., Gao, X., Santos, C. d. l., Live, D., and Patel, D. (1991) *Biochemistry 30*, 9022−9030.
15. Radhakrishnan, I., and Patel, D. (1992) *J. Am. Chem. Soc. 114*, 6913−6915.
16. Radhakrishnan, I., Patel, D., and Gao, X. (1992) *Biochemistry 31*, 2514−2523.
17. Coman, D., and Russu, I. M. (2002) *Biochemistry 41*, 4407−4414.
18. Wang, E., Malek, S., and Feigon, J. (1992) *Biochemistry 31*, 4838−4846.
19. Gowers, D. M., and Fox, K. R. (1997) *Nucleic Acids Res. 25*, 3787−3794.
20. Cantor, C. R., Warshaw, M. M., and Shapiro, H. (1970) *Biopolymers 9*, 1059−1077.
21. Marky, L. A., Blumenfeld, K. S., Kozlowski, S., and Breslauer, K. J. (1983) *Biopolymers 22*, 1247−1257.
22. Marky, L. A., and Breslauer, K. J. (1987) *Biopolymers 26*, 1601−1620.
23. Soto, A. M., and Marky, L. A. (2002) *J. Am. Chem. Soc.* (submitted).
24. Rentzeperis, D., Kharakoz, D. P., and Marky, L. A. (1991) *Biochemistry 30*, 6276−6283.
25. Rentzeperis, D., and Marky, L. A. (1995) *J. Am. Chem. Soc. 117*, 5423−5424.
26. Plum, G. E., and Breslauer, K. J. (1995) *J. Mol. Biol 248*, 679−695.
27. Record, M. T., Jr., Woodbury, C. P., and Lohman, T. M. (1976) *Biopolymers 15*, 893−915.
28. Krakauer, H. (1972) *Biopolymers 11*, 811−828.
29. Kiessling, L. L., Griffin, L. C., and Dervan, P. B. (1992) *Biochemistry 31*, 2829−2834.
30. Zimmer, C., Luck, G., Venner, H., and Fric, J. (1968) *Biopolymers 6*, 563−574.
31. Leitner, D., Schroder, W., and Weisz, K. (2000) *Biochemistry 39*, 5886−5892.

BI026166P